Bistatic SAR image formation

G. Yates, A.M. Horne, A.P. Blake and R. Middleton

Abstract: Synthetic aperture radar (SAR) allows all-weather, day-and-night surface surveillance and has the ability to detect, classify and geolocate objects at long stand-off ranges. Bistatic SAR, in which the transmitter and the receiver are on separate platforms, is seen as a potential means of countering the vulnerability of conventional monostatic SAR to electronic countermeasures, particularly directional jamming and avoiding physical attack of the imaging platform. As the receiving platform can be totally passive, it does not advertise its position by RF emissions. The transmitter is not susceptible to jamming and can, for example, operate at long stand-off ranges to reduce its vulnerability to physical attack. This paper presents part of the work undertaken at QinetiQ examining the techniques and additional complications involved in producing high-resolution bistatic SAR imagery. The work presented here focuses on a fully airborne, synchronised bistatic SAR demonstration using QinetiQ's enhanced surveillance radar and the Thales/QinetiQ airborne data acquisition system, which took place in September 2002. Some of the bistatic imagery from the trial are presented here and compared and contrasted with the monostatic imagery collected at the same time.

1 Introduction

The first radars were bistatic continuous wave devices, often using a transmitter of opportunity. They remained in a bistatic configuration until advances in engineering allowed the high-power transmitter and sensitive receiver to be collocated. Since then, the monostatic radar configuration has become established as the more practical system for most applications. Advances in timekeeping, communications and navigation in the last two decades have made bistatic radar a practical option again and bistatic systems have started to receive consideration for particular applications. A typical example of such work was the extensive research and demonstration programme into ground-based air defence radar, centred at what was then RSRE Malvern, and involving many research groups in UK industry [1].

Synthetic aperture radar (SAR) is becoming increasingly important in many military ground surveillance and targeting roles. This is because of its ability to operate in all weather, day-and-night and to detect, classify and geolocate objects at long stand-off ranges. SAR in UK is typified by the forthcoming airborne stand-off radar system [2]. Bistatic SAR, in which the transmitter and receiver are on separate platforms, is seen as a potential means of countering vulnerability to electronic countermeasures, particularly directional jamming, and avoiding physical attack of the imaging platform. As the receiving platform can be totally passive, it does not advertise its position by RF emissions. The transmitter is not susceptible to jamming and can, for example, operate at long stand-off ranges to reduce its vulnerability to physical attack.

IEE Proceedings online no. 20045091

doi:10.1049/ip-rsn:20045091

Paper first received 30th September 2004 and in final revised form 11th July 2005

The authors are with QinetiQ Ltd., St. Andrew's Road, Malvern, Worcestershire, WR14 3PS, UK

E-mail: gayates@QinetiQ.com

The first results of an airborne bistatic SAR demonstration were published in 1984 by Auterman [3]. In his experiments both aircraft were constrained to flying parallel flight paths. More recent practical work on the topic has seen successful bistatic SAR experiments using two airborne platforms by ONERA/DLR in experiments carried out in February 2003 [4–6] and by FGAN in November 2003 [7]. In both these sets of experiments, the aircraft are again constrained to flying nominally parallel trajectories.

This paper describes part of a programme of research funded under the MOD Corporate Research Programme, and undertaken by QinetiQ, Malvern. It is an extended version of a paper published at EUSAR 2004 [8]. It follows on from a previous paper entitled 'Bistatic synthetic aperture radar' presented at Radar 2002 in Edinburgh, UK [9]. That paper gave an overview of early theoretical work undertaken as part of a research programme by QinetiQ focusing on the processing techniques for bistatic SAR. This paper concentrates on the results from a fully airborne bistatic SAR demonstration. This used the spotlight mode of operation in which both radar beams are steered on to a pre-agreed spot on the ground, with no restrictions on aperture time. This removes the need for pulse-chasing techniques in which the receiver's beam is scanned to follow the moving beam from the transmitter [10], although these and the sophisticated antenna techniques needed to achieve them have been addressed elsewhere within the programme. In these experiments, the two aircrafts are not constrained to flying in formation. In fact, the aircraft are tens of kilometres apart with non-parallel trajectories, often providing bistatic SAR images from squinted geometries.

2 Bistatic SAR demonstration

2.1 Initial ground tests

Synchronisation (in both time and frequency) is a fundamental part of any bistatic radar system and is very demanding in bistatic SAR because of the long integration

times and wide signal bandwidths involved. There are two fundamental approaches to achieving bistatic synchronisation: provision of extremely accurate independent time and frequency standards on each platform, or the continuous transfer of time and frequency standards between platforms [10]. The first method requires some hardware such as an atomic clock. The second can be achieved through direct path reception of the transmitted waveform at the receiver, a dedicated RF link, or a broadcast link such as that provided by the GPS system. As stated in [9], within the scope of this work, synchronisation was achieved using a pair of caesium atomic clocks. Hardware modifications had to be made to each of the radars to incorporate a clock. These hardware modifications were tested in trials using both radars together on the ground.

Experiments were carried out using ESR as the transmitter with ADAS as the receiver in positions up to 1 km away. The radars were shown to be synchronised in time as consecutive pulses were recorded in the same range gate of the receiving window. This can be seen in the range compressed data shown in Fig. 1, where the peak in each pulse remains in the same range bin over successive pulses. An example of a single range profile taken from the ground trial is shown in Fig. 2. Here, the radars were approximately 600 m apart and the sidelobe levels are relatively high (about 22 dB down from the mainlobe), this can be explained by multipath effects as both radars were operating close to the ground. The radars were shown to be synchronised in frequency as the data could be range-compressed and the phase noise examined.

Fig. 3 shows the phase noise from the ground trial. The plot on the left-hand side is the monostatic phase noise from ADAS working in its conventional monostatic mode. The plot on the right-hand side shows the bistatic phase noise using ESR transmitting to ADAS. Both plots are centred around DC relative to the carrier frequency. The peak at DC shows that the oscillators are phase-locked. The overall phase noise floor has been raised by about 10 dB using different transmit and receive chains. The bistatic phase noise is considerably higher in the close-to-carrier region around DC, as the theoretical work predicted [9]. This is because in a monostatic system, low frequency components of phase noise have little effect on system performance because they change little from the time of pulse transmission to the time of reception. This time is of the order of the pulse repetition interval for a typical system, thus, the system is not susceptible to phase noise components at frequencies lower than the PRF. In the bistatic system, separate oscillators are used in the transmitter and the receiver and will exhibit independent realisations of phase noise. Thus, the bistatic system is susceptible to the whole phase noise spectrum, including the close-to-carrier component [3].

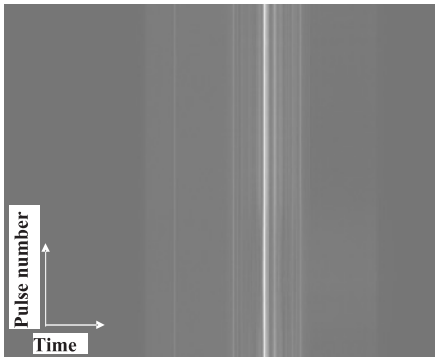

Fig. 1 *Range compressed data from ground trial*

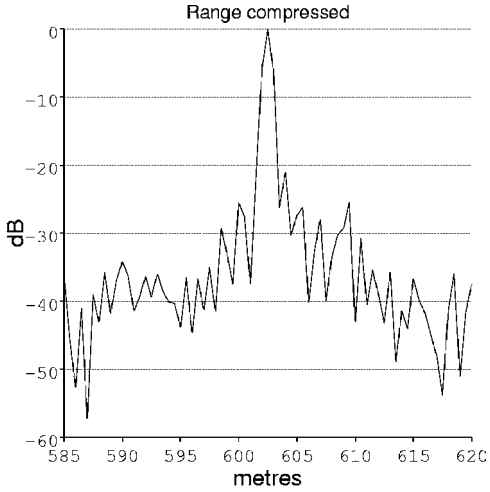

Fig. 2 *Range point spread function from the ground experiments*

2.2 Airborne demonstration

The experiment made use of the high transmit power of ESR (onboard a BAC1-11) with ADAS (on a helicopter) as the passive receiver. Both platforms operated in spotlight mode, imaging an urban environment surrounded by natural clutter regions. The radars were operating at the same X-Band centre frequency and using the same wide bandwidth. Data were recorded at a number of different imaging geometries, with the aim of investigating the effect of varying bistatic angle grazing angle and platform velocity on bistatic imagery. A schematic showing an example of a bistatic geometry indicating the bistatic angle is shown in Fig. 4.

2.2.1 Data processing: Within the scope of this work both the polar format algorithm (PFA) [11], and the range migration algorithm (RMA) [11], have been analysed as possible bistatic SAR processing routines. The monostatic PFA uses three key processing stages: compensation of the raw data for the motion of the imaging platform seen at scene centre; mapping of the resulting (approximate) polar K-space data onto a rectangular K-space representation; and a Fourier transform to the image domain. For this bistatic variant, the motion compensation to scene centre has been extended to include the motion of both the transmitter and receiver. The second stage has been adapted for bistatic geometries using an optimisation technique. The resulting scene size limitations (a known drawback of the PFA) appear to be comparable with those from the monostatic PFA.

To adapt the monostatic RMA for bistatic geometries, simplifications need to be made. This detracts from the attraction of the monostatic RMA's being an exact solution (subject only to the stationary phase approximation) and thus suffering no scene size limitations. The simplifications that need to be made in order to introduce bistatic geometries will introduce scene size limitations. This has not been investigated fully under this programme, but it is thought that these limitations would be similar to those introduced using the bistatic variant of the PFA.

The bistatic variant of the PFA was incorporated into a fully versatile processor. The processor is completely independent of the radars used and the trajectories of the two platforms. It uses the platform trajectories and the raw

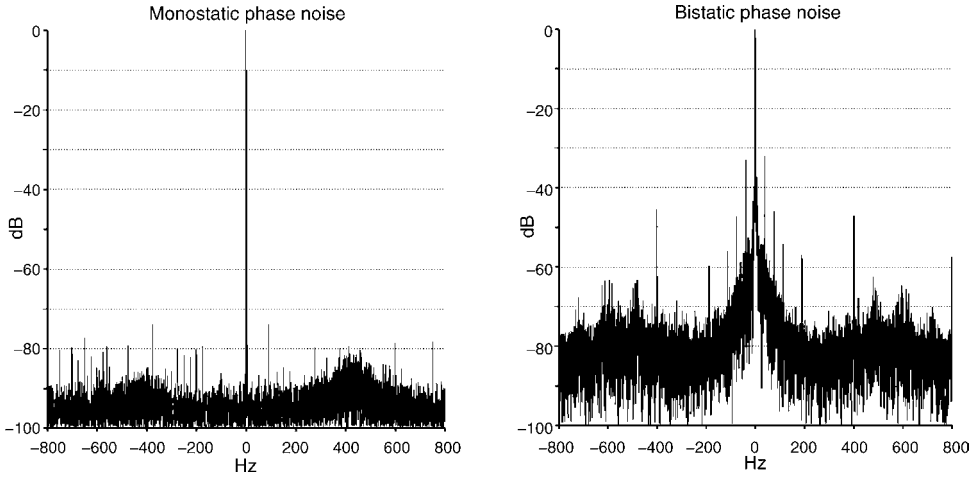

Fig. 3 *Phase noise, with power plotted against frequency, for monostatic (left) and bistatic operation*

data to form bistatic imagery. The processor has been written with all the functionality of a monostatic processor. The image is formed directly in the ground plane with the ability to use information from digital elevation models.

During the airborne trials, ADAS (the receiver) encountered problems recording data from its motion sensors. As a result of this the trajectory of ADAS was only known approximately and consequently errors were introduced into the bistatic imagery.

2.2.2 Autofocus: Owing to the motion-induced phase noise (particularly from the errors in the ADAS motion sensors) and the increased phase noise introduced using two radar systems, the trials data required autofocusing. Although research examined the development of a sophisticated model-based phase gradient algorithm (PGA) [12], autofocus which would be incorporated into the bistatic SAR processor, programme time constraints allowed only a simple stand-alone autofocus algorithm to be realised. This was based on the PGA, which exploits the fact that all scatterers are defocused by the same phase error. It estimates the phase perturbation of the brightest scatterer in each range bin of the image and combines them to maximise the signal-to-noise ratio in the phase error estimate. The data are corrected using the phase error estimate and the image is reformed. The process is repeated as necessary. A typical result from the autofocus can be seen in Fig. 5. The upper image is before autofocus, the lower image is after autofocus.

It is apparent from the images in Fig. 5 that some regions are better focused than others, and some types of structure are better focused than others. This is a result of the poor high-frequency performance owing to the approximations made in the autofocus. If better focused imagery is required, it will be necessary to study the geometry of bistatic SAR imaging and the nature of the autofocus to produce a more thorough and considered solution for bistatic imagery.

2.2.3 Bistatic SAR imagery: In all of the SAR imagery presented here, ESR is transmitting from the bottom right of the image. In the bistatic SAR images, ADAS is receiving from the bottom left of the image, as illustrated in the

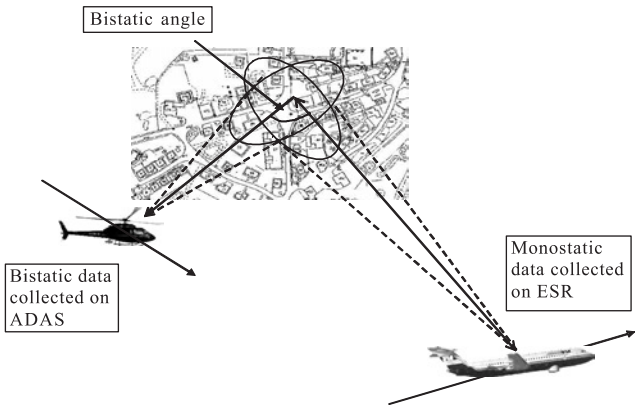

Fig. 4 *Schematic of bistatic imaging*

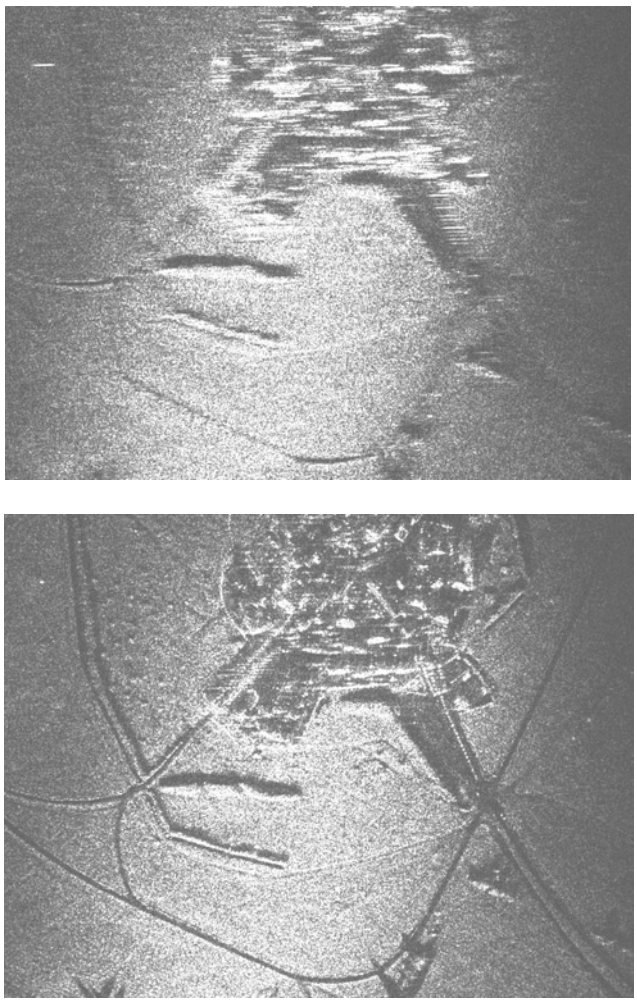

Fig. 5 *Bistatic image before (top) and after autofocus*

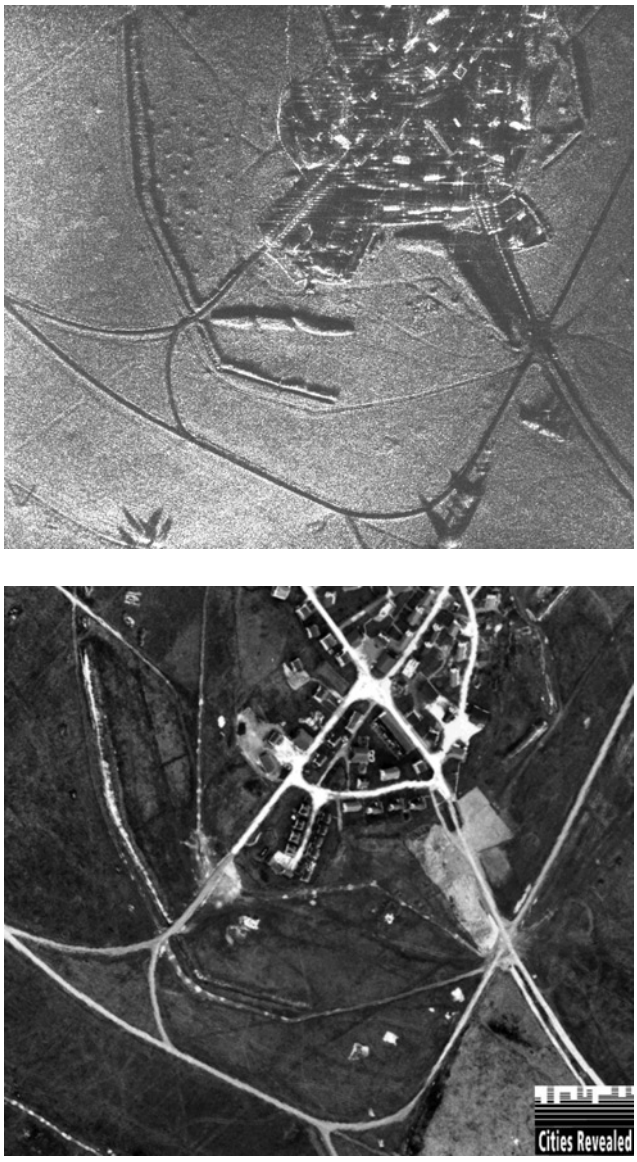

Fig. 6 *Bistatic SAR image with bistatic angle ~50° (top) along with aerial photograph of the region*
(Cities Revealed aerial photography © The GeoInformation Group)

schematic in Fig. 4. The bistatic imagery has had motion compensation and autofocus solutions applied. Fig. 6 shows a bistatic image with approximately 50° bistatic angle above an aerial photograph of the same region.

Towards the bottom of the bistatic SAR image in Fig. 6 there are some isolated tall trees from which it is possible to note the two shadows (one from the transmitter and one from the receiver). As the shadows are dark, it can be concluded that the phase noise and sidelobe levels are low. These dark shadows are particularly noteworthy considering the additional phase noise introduced using a different system to transmit and receive the radar signal. Also, the car park towards the bottom-right of the village appears dark. This too shows that the phase noise levels are acceptable.

The fences along the middle of the car park (bottom right of the image) and around the left of the urban area are clearly visible in the SAR image. It is easy to identify the tracks in the fields.

2.2.4 Bistatic SAR image characterisation and utility: For each of the bistatic images, the corresponding monostatic image can be formed from the data collected on ESR. The monostatic SAR imagery and the bistatic SAR imagery have been processed using different processors.

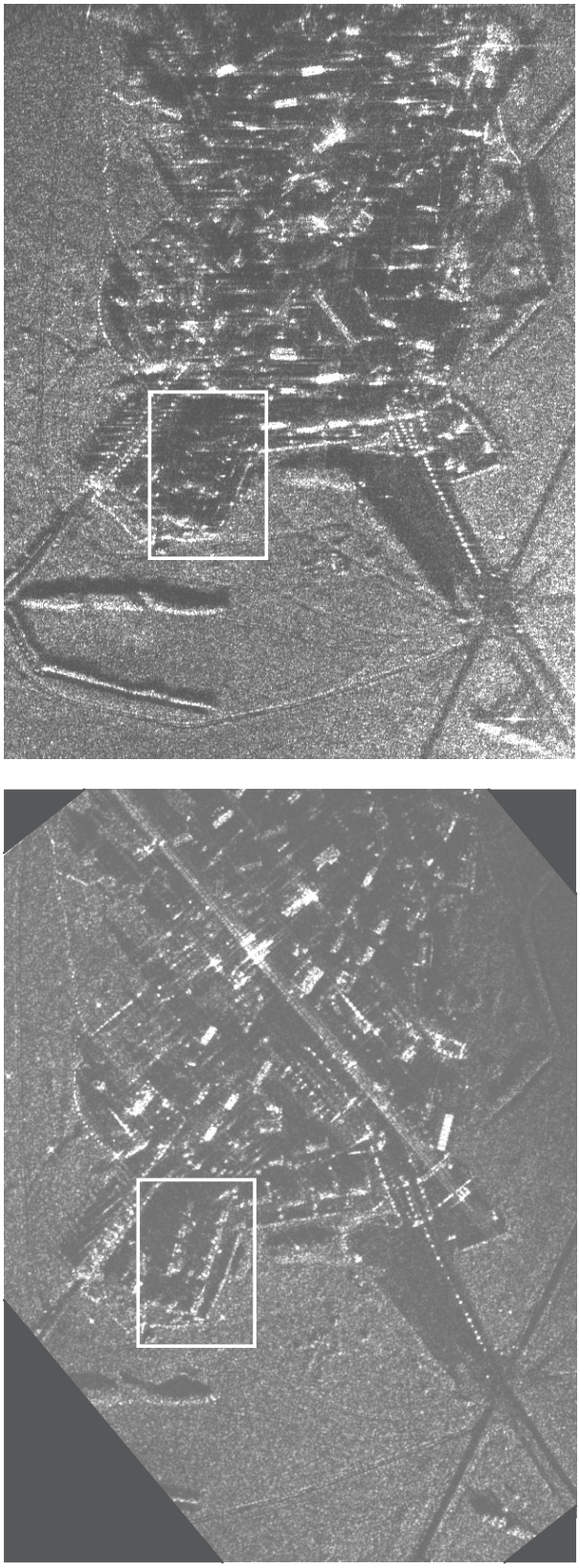

Fig. 7 *Bistatic image with ~70° bistatic angle (top) with corresponding monostatic image*
The same street is marked in both images for discussion

Fig. 7 shows a comparison of a bistatic SAR image (with bistatic angle of approximately 70°) above with the corresponding monostatic image. The monostatic image

has been formed from the monostatic data collected on ESR at the same time as the bistatic data were collected on ADAS. The monostatic image has been processed to the same resolution, without the use of autofocus. This is possible mainly because the navigation data on the BAC1-11 were accurate, but also because the single oscillator used in the monostatic system resulted in less phase noise in the image. The monostatic image has been rotated to be orientated along the same bearing as the bistatic one. In both images a row of houses has been marked for discussion later in this section.

The main observation is that, at a superficial level, the images appear quite similar. There are, however, differences in the scattering mechanisms in the two images. The monostatic image has a large flash from one of the buildings. This flash is not present in the bistatic image. This is likely to result from the man-made environment being made up of large numbers of trihedral and dihedral reflectors. These are more likely to act like retro-reflectors (directly reflecting energy back towards the emitter) and can produce large flashes, often obscuring weaker scatterers in monostatic imagery [9]. This effect is also demonstrated by the trihedral point targets that were placed around the village. These can be seen to the bottom-left of the village in the monostatic image but are not visible in the bistatic one.

More of the bistatic image is in shadow than the monostatic image. The additional shadowing can best be seen from the two mounds of earth, one towards the bottom and one to the right of the image. The shadowing from the buildings towards the top of the image is the same in both images as they are shadows from ESR. The effect of the shadowing on a target could be used to gain more information towards classifying a target. However, it is more likely that the two shadows would obscure other important scattering events. Two obvious ways of reducing the amount of shadow in the bistatic image are to reduce the bistatic angle (making the shadows overlap) or to increase the grazing angle.

Different buildings appear bright in the two images. The different scattering effects are noticeable on the row of dormer houses extending towards the bottom left of the image. This row of houses has been marked by a white rectangle in both images in Fig. 7. In the bistatic image the scattering is from the side of the dormer window, whereas in the monostatic image the whole of the roof is visible.

The fact that the images appear to be so similar implies that existing equipment and software available for utilising the images operationally may require little upgrading, but this needs to be fully investigated.

Another comparison of the two images is provided by analysing the clutter statistics. Three grass fields have been used which appear in both the bistatic and monostatic images. The goodness-of-fit of the probability distribution is given as a Kolmogorov–Smirnoff test probability. The distributions that have been fitted to the data were the negative exponential, the Weibull, the log-normal and the K-distributions.

In each of the three cases both the monostatic and bistatic clutter are best described by the K-distribution. This can be seen by the table of average probabilities shown in Table 1. The summary of the goodness-of-fit and the shape parameter of each K-distribution are shown in Table 2.

This shows that the goodness-of-fit is dependent on the particular data used. The value of ν, the shape parameter, is broadly similar throughout all the fields for both monostatic and bistatic data. The shape parameter is lower in the monostatic case that is the clutter appears spikier.

Table 1: Average Kolmogorov–Smirnoff test fit probability results for three fields

	Negative exponential	Weibull	Log-normal	K
Monostatic	9.1×10^{-27}	2.6×10^{-03}	3.0×10^{-68}	0.5
Bistatic	2.4×10^{-44}	1.6×10^{-04}	1.8×10^{-109}	0.6

Table 2: K-distribution for clutter comparison

	Monostatic		Bistatic	
	Fit probability (%)	ν	Fit probability (%)	ν
Field 1	16	4.27	80	10.1
Field 2	72	6.02	58	6.25
Field 3	46	4.10	44	5.64

This implies that point-target detectors could be more sensitive in the bistatic imagery, provided that the targets have the same characteristics as in monostatic imagery.

3 Conclusions and future work

We have demonstrated high-resolution, airborne bistatic SAR imagery. This uses two airborne platforms flying completely arbitrary flight tracks. There is no requirement for constrained trajectories.

This is of major importance to UK surveillance and targeting programmes. It allows critical all-weather, long-range target detection, classification and precision location capability to be maintained in the presence of physical and electronic countermeasures.

Bistatic imagery of targets has been examined. A study into the characterisation and utility of bistatic SAR images has been initiated using both the real and simulated data. This initial work has shown that, at a high level, the images appear similar to the monostatic ones.

Ongoing work includes a bistatic turntable ISAR experiment using military and civilian vehicles as targets. It is hoped that the results from this will allow a greater understanding of the scattering mechanisms of bistatic imaging. It may be possible to use the bistatic scattering mechanisms, for example, the lack of bright trihedral reflections and the two shadows, to gain additional target information from bistatic SAR imagery not available in the monostatic SAR image.

To gain a greater understanding of the scattering mechanisms in bistatic imaging, planned work also includes calculating bistatic RCS measurements of both the clutter and urban regions using the bistatic SAR imagery. In addition, the use of simulations will be examined with models of urban areas as well as high-fidelity vehicle models.

4 Acknowledgments

This work was sponsored by the United Kingdom MOD Corporate Research Programme under the ES domain.

5 References

1 Dunsmore, M.: 'Bistatic radars', in Galati, G. (Ed.): 'Advanced radar techniques and systems' (Peter Peregrinus Ltd, 1993), pp. 890–912
2 Streetly, M.: 'Airborne StandOff Radar (ASTOR) Programme'. Jane's Electronic Mission Aircraft 02, 15 January 1999
3 Auterman, J.L.: 'Phase stability requirements for bistatic SAR'. Proc. IEEE Nat. Radar Conf., Atlanta, March 1984, pp. 48–52

4 Wendlar, M., Krieger, G., *et al*.: 'Results of a bistatic airborne SAR experiment'. Proc. IRS 2003, Dresden, Germany, 2003, pp. 247–253
5 Dubois-Fernandez, P., *et al*.: 'Analysis of bistatic scattering behavior of natural surfaces'. Proc. EUSAR 2004 Conf., Ulm, Germany, May 2004, pp. 573–576
6 Cantalloube, H., Wendler, M., Giroux, V., Dubois-Fernandez, P., and Krieger, G.: 'Challenges is SAR processing for airborne bistatic acquisitions'. Proc. EUSAR 2004 Conf., Ulm, Germany, May 2004, pp. 577–580
7 Waterscheid, I., Brenner, A.R., and Ender, J.H.G.: 'Geometry and systems aspects for a bistatic airborne SAR experiment'. Proc. EUSAR 2004 Conf., Ulm, Germany, May 2004, pp. 567–570
8 Yates, G., Horne, A.M., Blake, A.P., Middleton, R., and Andre, D.B.: 'Bistatic SAR image formation'. Proc. EUSAR 2004 Conf., Ulm, Germany, May 2004, pp. 581–584
9 Horne, A.M., and Yates, G.: 'Bistatic synthetic aperture radar'. Proc. Radar 2002 Conf., Edinburgh, Scotland, October 2002, IEE Publication No. 490, pp. 6–10
10 Willis, N.J.: 'Bistatic radar' (Artech House, 1991), pp. 254–257
11 Carrara, W.G., Goodman, R.S., and Majewski, R.M.: 'Spotlight synthetic aperture radar' (Artech House, 1995)
12 Jakowatz, C.V., Wahl, D.E., Eichel, P.H., Ghiglia, D.C., and Thompson, P.A.: 'Spotlight mode synthetic aperture radar' (Kluwer Academic Publishers, 1996), pp. 251–269